Optimized Adsorption Heat Pump for Efficiency Increase of District Heating Networks

Emanuele Piccoli[1], Romain Civioc[1], Sandra Galmarini[1], Xavier Jobard[2], Alexis Duret[2], Xavier Daguenet[3] and Paul Gantenbein[3]

[1] Empa, Dübendorf (Switzerland)

[2] HEIG-VD, Yverdon-les-Baines (Switzerland)

[3] OST, Rapperswil (Switzerland)

Abstract

Adsorption heat pumps can provide cooling based on renewable district heat or waste heat, thus expanding the scope of district heating networks (DHN) and making better use of existing renewable heat sources. On the other hand, they can also provide heat while significantly reducing the return flow of the district heating network, thus increasing the efficiency of district heating supply. However, commercially available sorption machines are not designed for DHN. Therefore, new and sustainable adsorbent materials ideally suited for the temperatures and applications of district heating networks are developed and incorporated in a heat & mass exchanger designed for reversible adsorption heat pumps. The new sorption heat and mass exchanger is subjected to performance measurements. The results are used to carry out simulations to demonstrate the advantages of adsorption heat pumps for the supply of cooling and heating in district heating networks.

Keywords: Renewable heating and cooling, Adsorption heat pumps, Activated carbon adsorbent, Prototype testing, Energy system efficiency

1. Introduction

Due to climate change and the ensuing rise of the outdoor temperatures, the cooling demand in buildings will increase in the future (Birol, 2018). Nevertheless, the heating demand in Europe will remain high in wintertime (Settembrini et al., 2017). In order to achieve the energy turnaround for Europe and to reduce drastically greenhouse gas emissions, innovative, integrated and eco-friendly heating and cooling solutions are required to supply the building stock as well as processes with heating and cooling. On the one hand, the CO2 footprint of the energy mix during peak load in winter is high. On the other hand, during summer, large amounts of heat remain unused from waste incineration plants and other industrial processes because of the low heat demand during this season. In Switzerland, a large majority of Municipal Waste Incineration Plant (MWI) are connected to large DHN. This source of heat represents close to a third of the heat distributed in DHN in 2020[1]. The MWI typical efficiency combining heat and electricity production in 2020 is in average around 70%[2]. So 30% of the heat could still be valorized. The thermal losses are mainly occurring in summer time where the heat demand is low. The extra heat unused in summer time can be estimated to around 800Wh. This heat can be used in summer to power adsorption heat pumps (adHP) and supply eco-friendly and cost-effective cooling energy to various cooling consumers (e.g. buildings and industries) (Hassan et al., 2020).

District heating networks (DHN) are a well-known solution to lower the carbon footprint for heating in winter and recover otherwise unused waste heat (Puschnigg et al., 2021). However, DHN suffers from two important drawbacks, which limits their energy efficiency and operability: 1) Low efficiency caused by high operating temperatures, especially high return temperatures. 2) Low utilization of the DHN in summer time, which leads to inefficient operating conditions. The impacts of those two drawbacks are reduced heat distribution capacity for a given pipe diameter (due to limited temperature differences), high heat distribution costs (pumping energy and heat losses)

[1] https://www.fernwaerme-schweiz.ch/fernwaerme-franz/Verband/Jahresbericht.php
[2] https://vbsa.ch/donnees/energie-charts/?lang=fr

doi:10.18086/eurosun.2022.04.10 Available at http://proceedings.ises.org

and lower energy efficiency in the heating station (more energy to produce one unit of useful heat).

This work investigate the integration of reversible adsorption heat pumps into DHN to use untapped waste heat and increase the energy efficiency of district heating networks. Two particularly promising integrations of adHP in DHN have been identified. The DHN return temperature reduction operating mode (Figure 1 (a)) integrate an adHP at substations (SST) providing heat at the building level. The adHP uses the SST return flow as a heat source for the evaporator and thus reduces the temperature of the DHN return flow. This mode of operation increases the temperature difference between the forward and return of the DHN resulting saving on the pumping energy or in heat delivery capacity increase of a given thermal grid. Additionally, it also reduces heat losses since the return temperatures are lowered. The same adHP and the DHN heat supply can also supply comfort cooling (Figure 1(b)) to the buildings in summer time. This enables the DHN operators to offer a new energy service to their customers, while increasing the sale of heat in summer and thus the profitability of the DHN (40.8% and 31.8% of the heat distributed respectively)[3]. Since a major part of heat is either renewable or waste heat in Swiss DHN, this cold supply will also be renewable. The major challenge for this mode of operation is to dissipate and/or recover condensation and adsorption heat at intermediate temperature without extra cost, for with pre-heating of domestic hot water.

These innovative conceptual modes of operation have been evaluated separately with numerical models reflecting the current state of the art of the sorption technology and with experimental work carried out on commercial units by (Jobard et al., 2020). It results that the commercial units currently available are not adapted for integration in DHN and do not meet the requirements of DHN operators, especially in terms of temperature drop at the desorber in cooling mode. They suffer also from low power density and low thermal efficiency. Therefore, new adsorption materials are needed as well as new concept for reversible DHN SSTs for heating and cooling of buildings.

In this work, we move towards the design of such systems. In a first section, we analyze the requirements of the DHN applications based on surveys. Afterwards, we propose a novel sustainable adsorbent material suitable for the application and we analyze its performance by models and simulations. At last, we present the characterization methods to measure the performance of adHP prototypes.

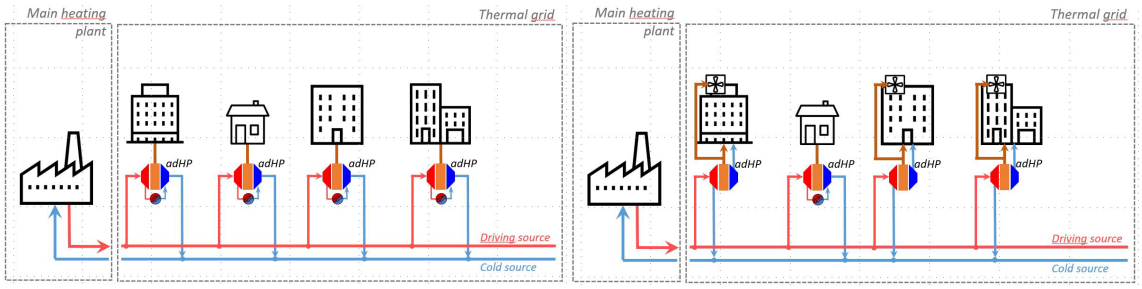

Figure 1 - Schematic view of the two applications of adHP in DHN targeted: a) return temperature reduction and b) cooling. The adHP are used in the substations to serve the DHN users.

2. DHN implementation requirements

This section presents the requirements necessary to drive the development and optimization of the adsorption materials for DHN applications. These requirements are the expected operating conditions for both heating and cooling modes. These conditions are defined with the T_{hot}, T_{con} and T_{eva}. T_{hot} is directly set from the supply of the DHN, T_{con} depends on the space heating and domestic hot water distribution system; T_{eva} depends on the space heating return temperature and on the cooling distribution system (radiant ceiling or air conditioning unit), respectively in heating mode and cooling mode. Their ranges were derived from field surveys as well as from discussion with DHN operators and are gathered in Table 1.

In the heating mode, the purpose of the substation is to satisfy the building needs in space heating and domestic hot water. The adHP is implemented in this configuration to reduce the return temperature to the grid. Therefore, the DHN efficiency and capacity are improved. The Figure 2 present the simplified hydraulic of the substation. In this mode, the DHN drives the adHP at a given temperature T_{hot} and supplies heat to the space heating loop via the

[3] https://www.fernwaerme-schweiz.ch/fernwaerme-franz/Verband/Jahresbericht.php

heat produced at the adsorber and condenser of the adHP. A heat exchanger is present to cool down the heat carrier from the desorber below the condensing temperature. This is possible with low space heating return temperature. For this to function the adsorption temperature T_{ads} must be higher than T_{con}.

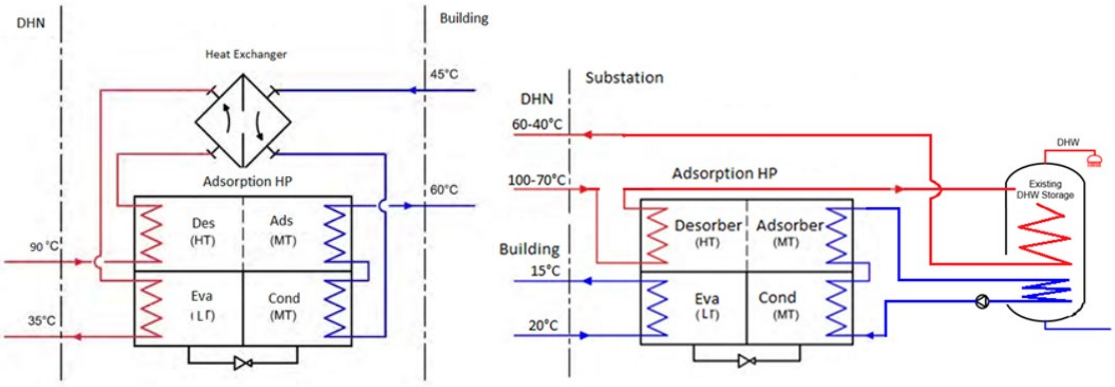

Figure 2 - Simplified hydraulic diagrams with example of possible temperature levels of each loop for the heating mode (left) and the cooling mode (right)

For implementation in existing DHN, the substation has to follow prescription given by the operators of the network that ensure a coherent integration and the supply temperature is fixed. Since DHN must supply temperature high enough for Domestic Hot Water (DHW) preparation at 60°C, as reported by (Quiquerez, 2017) supplied temperature are usually above 70°C and smaller than 110°C. Higher temperatures might in general be needed improve the COP of the machine and cooling power at the evaporator, especially considering that the desorption temperature must be below the hot source temperature to guarantee effective heat transfer. However, selecting the right adsorbent material can guarantee successful desorption. The temperature for the space heating loop is given by the characteristics of the building i.e., its energy standard and heat emission system. High temperature radiators with temperature need above 60°C are excluded because the needed temperature is to close from the supply temperature. Supply temperature of the space heating loop can be as low as 30°C for floor heating system in well insulated buildings. The evaporating temperature depends on the space heating return temperature and the pinch of the heat exchanger assumed at 5K. These are estimated with the temperature drop possible in the space heating loop. For radiators with supplied temperature of 65°C, a temperature drop of 10K and a pinch 5K induces a temperature at the evaporator inlet of 50°C. For floor heating, the temperature drop can only be of 5K, resulting in 20°C.

In the cooling mode, the adsorption pump in the substation is used to cool down buildings. In order to be able to operate in cooling mode without dry cooler to get rid heat rejection, different strategies have to be evaluated in order to valorize the rejection heat locally. One of the most promising local application for heat rejection valorization is DHW preheating. Alternatively, the heat rejected could be used as cold source for a heat pump for DHW preparation. The challenge with this local heat valorization is that the DHW need consumption affects the amount of cooling which can be produced by the AdHP. In order to operate successfully AdHP using heat supplied by a DHN, it is necessary to enlarge the temperature difference on the primary side and simultaneously to use heat at the lowest possible temperature. This represents a challenge as most of the adsorption chiller commercially available today are operated with a maximum 5°C difference and needs heat at minimum 60-65°C. This application could be interesting for DHN operators. It will intensify the heat demand in summer time when the DHN infrastructure are underused. Moreover, as most of DHNs today use a large fraction of renewable heat in their energy mix, this new application will make available renewable heat in dense urban area.

Figure 2 shows a possible hydraulic integration of an AdHP in cooling mode in a substation where the heat rejected is valorized to preheat DHW. This configuration is interesting as it eliminates the need of a dry cooler. On the other hand, it has to be operated with an important constraint: there must simultaneously cooling and DWH. Consequently, it will not be possible to produce cooling when there is no DHW demand. A compression HP could be integrated between the heat rejected by the AdHP and the DHW tank to give a bit more operating flexibility.

The Table 1 shows the operating conditions of the AdHP in cooling mode. Those conditions are derived from exchange with various DHN operators. The cooling is produced between 6 and 15°C. The forward temperature

must be at least 60°C in order to reduce too much the cooling COP. In addition, as mentioned above, it is important to insure a large temperature difference between the DHN forward and return stream for not deteriorating the DHN distribution losses and pumping energy consumption.

Table 1 - DHN temperature requirements in heating and cooling modes.

Scenario	Heating Mode			Cooling Mode		
	T_{hot}	T_{con}	T_{eva}	T_{hot}	T_{con}	T_{eva}
min-max	343-383 K	303-338 K	293-323 K	333-363 K	303-338 K	279-288 K

3. Adsorbent Material Development

Current state-of-the-art activated carbons (AC) are synthesized mostly by a bottom-up approach using toxic chemicals such as resorcinol and formaldehyde to form porous networks (Alshrah et al., 2017) which are then pyrolyzed and activated (Huber et al., 2016). The corresponding activated carbons can display a variety of microstructures and properties, making them interesting for different applications – including water sorption (Civioc et al., 2020; Huber et al., 2019). In the existing literature, green alternatives to petroleum-derived phenolic networks have been thoroughly studied to great avail (Nowicki et al., 2010; Prauchner and Rodríguez-Reinoso, 2012). However, none of them displays the array of properties required in our current work (e.g. able to adsorb and desorb in both heating and cooling mode).

Therefore, we herein study an alternative starting material: an activated carbon derived from spent coffee grounds (SCG). The properties and microstructure of the corresponding pyrolyzed material, arising from a more sustainable feedstock (thus greatly improving the carbon footprint of the adsorption heat pump) are studied. Its water adsorption characteristic is comparable with the one from more traditional resorcinol-based activated carbons; retaining an optimal performance is crucial for the efficiency of the project overall.

However, one of the main advantages of traditional resorcinol-based ACs is their monolithicity; they can be tailored thanks to the bottom-up synthesis approach by pouring the sol into a box of the desired shape. In this regard, SCG are more restrictive because of their granulated nature. Therefore, in this work we opted for a minimal usage of resorcinol and formaldehyde as a binder, effectively forming a matrix around SCG. It allows the materials to reach a monolithic state while being mostly sustainable. Importantly, this does not compromise the water adsorption performance of the materials.

Our synthesis protocol involves the collection of spent coffee grounds, which are then mixed with a minimal amount of resorcinol and formaldehyde. Typically, 30g of dry SCG and 25 mL of ethanol are mixed with 6g of resorcinol and 12 mL of commercial formaldehyde aqueous solution. A catalytic amount of ammonia in the form of an aqueous solution, around 1 mmol, is then added to the mixture. It is then poured into polypropylene boxes of the desired shape. The materials are left to cure and dry in a convection oven before being pyrolyzed and physically activated in a one-step heat treatment within a tube furnace – at 800 °C for 4 hours under a CO2 atmosphere. The result is a monolithic activated carbon, depicted in Figure 3, which can be characterized as necessary and is ready for water sorption applications.

As a finer particle size of the AC could be beneficial from the mechanical standpoint, it was decided to test the AC obtained from the fraction of the green body with the smaller diameter. Before synthesis, SCGs were sieved and only the fraction whose diameter did not exceed 200 micrometers was used – resulting in a drastic improvement of the adsorption characteristic (60% more water capacity) , as visible in Figure 4. This result, which surpasses the state-of-the-art carbons, opens very promising applications and should be further investigated, especially given the low desorption temperatures required. However, the material evaluation was performed on the basis of the more complete information available for the AC obtained from the not sieved SCG.

The ACs are currently sporting a slab shape. Therefore, envelope density ρ_{env} was calculated using a caliper to measure the dimensions of the materials. Subsequently, skeletal density ρ_{skel} was measured by means of helium pycnometry (Accupyc, Micromeritics). This calculations allows for the determination of the entirety of the pore volume within the materials, including their microporosity mesoporosity, and macroporosity (d > 50 nm) without further quantitative information.

The porosity of those materials was further characterized using nitrogen physisorption and carbon dioxide physisorption. For nitrogen sorption, an NLDFT kernel based on (Tarazona, 1985) was chosen. For CO2 sorption, an NLDFT kernel based on (Olivier, 1995) was used. The as-obtained isotherms are subsequently merged using the 3Flex software from Micromeritics. Thus, the microporosity v_μ (diameter < 2nm) and mesoporosity v_m (2 nm < diameter < 50 nm) of the materials was characterized both qualitatively and quantitatively, assuming respectively a slit and a cylindrical geometry. The amount of macroporosity was then determined by subtracting those two values from the total pore volume calculated as in Eq. 1. The volumetric pore fraction of the material ε can be then calculated as in Eq. 2.

$$v_t = \frac{1}{\rho_{env}} - \frac{1}{\rho_{skel}} \qquad \text{Eq. 1,} \qquad \varepsilon = v_t \cdot \rho_{env} \qquad \text{Eq. 2}$$

The wet thermal conductivity k_{50} of the ACs was determined using a custom-made guarded hot plate device (Stahl et al., 2012) at 30 °C and 50% relative humidity. Finally, dynamic water sorption isotherms were recorded on an isothermal gravimetric device (VTI-SA+ Water Vapor Sorption Analyzer, Porotec) between 5% and 80% relative humidity. For the ACs under analysis, the water adsorption characteristic be described following the Dubinin-Astakhov model (Dubinin and Astakhov, 1971):

$$w = W \cdot \exp\left(-\left(\frac{F}{C}\right)^N\right) \qquad \text{Eq. 3,} \qquad F = -\frac{R}{M} \cdot T \cdot \ln\left(\frac{p}{p_{sat}}\right) \qquad \text{Eq. 4}$$

The results are gather in Table 2. For the sieved SCG+RF AC, the water adsorption parameters were found to be $W = 0.48$, $C = 186$, $N = 2.4$, which means that the total capacity was enhanced without changing the type of adsorption sites.

The thermophysical properties of the AC strongly influence the performance of the adHP. To estimate the achievable performance of the SCG-based adsorbent monoliths, a dynamic model was used to calculate the energy efficiency and the power that the materials can deliver under the working conditions defined in Section 2. The model was developed in OpenModelica, following the lumped-parameter approach described in (Piccoli et al., 2021). Using such an approach assumes that the global adsorption dynamic can be sufficiently well described as if happening a single effective thermodynamic state (temperature, pressure, loading), instead of simulating all the local thermodynamic states developing within the adsorbent. Such a model includes only the heat and mass transfer within the material itself, therefore can be used as a term of comparison for different materials, boundary conditions and geometries, and not as a reference for whole adHPs.

The model is composed by a temperature boundary condition (representing the HEx fin temperature), a heat transfer resistance (representing the conduction within the AC), a heat and mass balance (representing the adsorption reaction in the pores), a mass transfer resistance (representing the vapour diffusion in the pores), one pressure boundary conditions (representing the evaporator/condenser). All these elements are connected in this order, such that the adsorption dynamics calculated in the heat and mass balance depend on the materials properties and on the boundary conditions.

Figure 3 – SCG+RF monoliths before (left) and after (right) pyrolysis

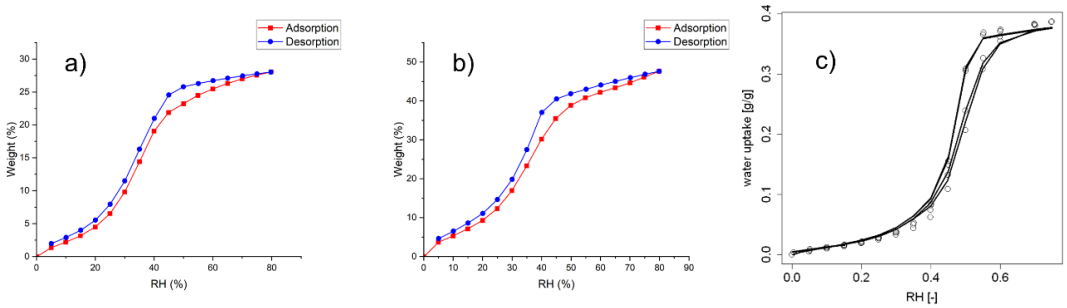

Figure 4 – Water adsorption isotherms at 30°C of not sieved (a) and sieved (b) SCG+RF AC and of RMF AC (c).

Table 2 – Thermophysical properties of the SCG+RF AC monoliths

Property	ρ_{env}	ρ_{skel}	v_M	v_m	v_μ	ε	k_{50}	W	C	N
Value	0.56 [g/cm³]	1.6 [g/cm³]	0.83 [cm³/g]	0.03 [cm³/g]	0.30 [cm³/g]	66 [%]	0.092 [W/m/K]	0.29 [g/g]	185 [J/g]	2.6 [ ]

The temperature and pressure boundary conditions are modelled as square waves oscillating between the adsorption and the desorption heat transfer fluid temperatures and evaporator and condenser pressure, respectively. Moreover, a control mechanism forbids flow reversal for the pressure boundary condition.

The heat transfer resistance R_{heat} within the monolith is modelled as transient 1-D conduction:

$$R_{heat} = \frac{(2 \cdot s)^2}{\pi^2 \cdot \alpha \cdot V_t \cdot c \cdot \rho_{env}} \cdot \left(1 - 0.3 \cdot \exp\left(-\frac{\tau}{8.9e-4}\right) - 0.7 \cdot \exp\left(-\frac{\tau}{1.3e-2}\right)\right) \quad \text{Eq. 5}$$

The adimensional time τ, determining the transient term, is the equivalent of the Fourier Number in absence of adsorption. However, the adimensional time is stretched due to the additional adsorption energy terms in the heat balance and by its entanglement with the mass transfer. To compensate for this, it is implicitly extracted from the state of the material:

$$\frac{T - T_i}{T_f - T_i} = 1 - 0.82 \cdot \exp\left(-\frac{\tau}{1.0e-1}\right) - 0.18 \cdot \exp\left(-\frac{\tau}{4.6e-3}\right) \quad \text{Eq. 6}$$

Similarly, the mass transfer resistance within the monolith is modelled as microscopic surface diffusion and a transient 1-D macroscopic diffusion:

$$R_{mass} = \frac{r_\mu}{3 \cdot D_\mu \cdot \rho_{env} \cdot s \cdot a_{surf} \cdot A_s} + \frac{s}{D_{M*} A_s} \cdot \left(0.3 \cdot \exp\left(-\frac{\tau}{8.9e-4}\right) - 0.7 \cdot \exp\left(-\frac{\tau}{1.3e-2}\right)\right) \quad \text{Eq. 7}$$

Eq. 3 implies that the size of the bigger porosity is not limiting the gas mean free path and therefore no major difference among more or less porous materials should be expected. Furthermore, given the characteristic lengths at play in the microscale and in the macroscale ($r_\mu \sim 1\ \mu m$ and $s \sim 1\ mm$) the macroscopic diffusion is by far the limiting mechanism, especially at low values of τ. This is similar to the trends observed for coatings (Ammann et al., 2019).

In Eq.1, Eq. 2 and Eq.3 the exponential equations are numerically derived from the analytical solutions (Carslaw and Jaeger, 1959) of the average thermal resistance and of the average temperature of infinite slabs, respectively. It can be noticed how the transient term of the heat and mass transfer resistances are complementary. The reason is that the effective state of the material represents also the position in the monolith in which the adsorption is occurring. At the beginning of each step, the adsorption is temperature driven, so it happens at a minimum distance from the fin surface and at a maximum distance from the vapour interface (R_{heat} is small and R_{mass} is big), while at the end of the step, the opposite will happen.

The essence of the heat and mass balance consists in two equations, entangled by the water loading w:

$$\frac{T_f - T}{R_{heat}} + \dot{m}_v \cdot (h_{ext} - h_{int}) = (m_s \cdot c_s + m_a \cdot c_a) \cdot \frac{\partial T}{\partial t} - H \cdot m_s \cdot \frac{\partial w}{\partial t} + m_v \cdot \frac{\partial h_{int}}{\partial t} + h_{int} \cdot \frac{\partial m_v}{\partial t} \quad \text{Eq. 8}$$

$$\frac{\gamma_{ext}-\gamma_{int}}{R_{mass}} = \gamma_{int} \cdot \frac{\partial V_v}{\partial t} + V_v \cdot \frac{\partial \gamma_{int}}{\partial t} + V_t \cdot \rho_{env} \cdot \frac{\partial w}{\partial t} \quad \text{Eq. 9}$$

The state of the AC is determined by its properties, namely thermal diffusivity α, specific heat capacity c, envelope density ρ, thickness s and water adsorption characteristic $w = w(p,T)$. As stated above, one of the advantages of using ACs as adsorbent material is the possibility of tailoring their properties to a given application. In particular, for SCG this can be controlled by changing the pyrolysis process to have more or less microporosity and macroporosity. This will influence the adsorption characteristic, the density and the thermal diffusivity. In order to understand how the different pyrolysis conditions (CO_2 flowrate, max temperature and time above the critical temperature of the coffee) affect these properties, a Design of Experiment based on a central composite design was performed on the SCG. Regarding the adsorption characteristic and the density, we established that the flow of CO_2 does not have a significant influence within the range studied, while the maximum temperature and the pyrolysis time have a great influence. The thermal diffusivity, instead, strongly depends on the process of creation of the monolith from the AC powder. As this would add more parameters to the analysis, it was not included and the reference thermal conductivity of 0.067 W/m/K (obtained for a highly macroporous RMF AC monolith) was used instead. This means that the thermal resistance might be overestimated for the denser samples. Moreover, the specific heat capacity was assumed to be similar to the one measured for the RMF AC (Piccoli et al., 2021).

In general, each material property P can be described as a function of the maximum pyrolysis temperature $T \in [632{,}968\ °C]$ and the duration of the pyrolysis above 300°C $D \in [244{,}429\ min]$:

$$P = a \cdot T + b \cdot D + c \cdot T \cdot D + d \quad \text{Eq.10}$$

Table 3 summarizes the results obtained for the SCG AC powder.

Table 3 – Description of SCG AC properties as a function of the pyrolysis parameters

Material Property	Symbol [Units]	Temperature coeff. a	Time coeff. b	Temp./Time coeff. c	Constant coeff. d
Saturation Water Capacity	$W\ \left[\frac{g_w}{g_s}\right]$	0	-1.3e-3	2.4e-6	0
Char. Energy of Adsorption	$C\ \left[\frac{J}{g}\right]$	0.43	1.2	-2.0e-3	0
Ads. Curve Shape Factor	$N\ [-]$	0	0	0	2.0
Skeletal Density	$\rho_{skel}\ \left[\frac{g}{cm^3}\right]$	0	-2.1e-3	2.9e-6	1.7
Envelope Density	$\rho_{env}\ \left[\frac{g}{cm^3}\right]$	5.6e-4	1.4	2.4e-6	0

Given the requirements of DHN for heating and cooling purposes, the performance of the SCG ACs should be tailored accordingly. Therefore, we used the dynamic adsorption model to simulate the Key Performance Indicator (KPI) of the material in a range of process, material and application parameters. The KPI was selected to be a tradeoff between energy efficiency and specific cooling power reached by an adsorption/desorption cycle in steady state (i.e. after 50 cycles):

$$KPI_{heating} = \frac{(E_{con}+E_{ads})^2}{E_{hot} \cdot t_{cycle}} \quad \text{Eq. 11,} \qquad KPI_{cooling} = \frac{(E_{eva})^2}{E_{hot} \cdot t_{cycle}} \quad \text{Eq.12}$$

In order to ensure a feasible heat exchange to with the heat transfer fluid, the desorption temperature is assumed to be 5 K below T_{hot} and the adsorption temperature is assumed to be 5 K above T_{con}. To minimize the number of simulation required, the working temperatures $T_{eva}, T_{con}, T_{hot}$ were fixed to 293, 308, 368 K for the heating mode and to 288, 303, 363 for the cooling mode respectively. Firstly, the best pyrolysis conditions for the (improvable) not sieved SCG+RF AC were defined by calculating the KPI for long cycles (reaching full equilibrium). The best material was selected for 3 scenarios, for which the total KPI was calculated as $KPI_t = \left(\frac{\varphi_h}{KPI_{heating}} + \frac{\varphi_c}{KPI_{cooling}}\right)^{-1}$:

- Current Demand (CD), serving only heating, with $\varphi_h = 1, \varphi_c = 0$
- Moderate Cooling (MC), where the cooling demand is less important than the heating demand, with $\varphi_h = 0.67, \varphi_c = 0.33$
- High Cooling (HC), where cooling demand is as important as the heating demand, with $\varphi_h = 0.5, \varphi_c = 0.5$

The pyrolysis conditions delivering the ideal materials for the three scenarios are listed in Table 4. The material design is clearly limited by space in which they were investigated: higher temperature and lower duration of pyrolysis would be beneficial. Moreover, the cooling mode is by far the most constraining and it dominates the choice for MC and HC scenarios.

Table 4 – Optimal pyrolysis parameter for the different application scenarios

Parameter	Current Demand	Moderate Cooling	High Cooling
T	968 °C	968 °C	968 °C
D	275 min	244 min	244 min

For the investigation of the optimal material thickness and cycle time, the material for MC and HC was used. When simulating different monolith thicknesses, thinner materials were able to produce much higher power, and therefore preferred. For example, a thickness of 1 mm (one order of magnitude higher than conventional coatings), delivered maximum KPI with a full cycle time of about 25 s, that is at the limit of the capacity of conventional heat exchangers, which have important thermal inertia. This means that for thin coatings, work should be done towards fast heat exchangers design. For 2 mm monoliths, however, the ideal cycle time increase to 100 s, as shown in Figure 5. The achieved thermal coefficient of performance reached 0.79 and the $KPI_{cooling}$ 1.4 kW/kg. This means that the monolithicity of the adsorbent offers a great advantage in the design of the heat exchanger.

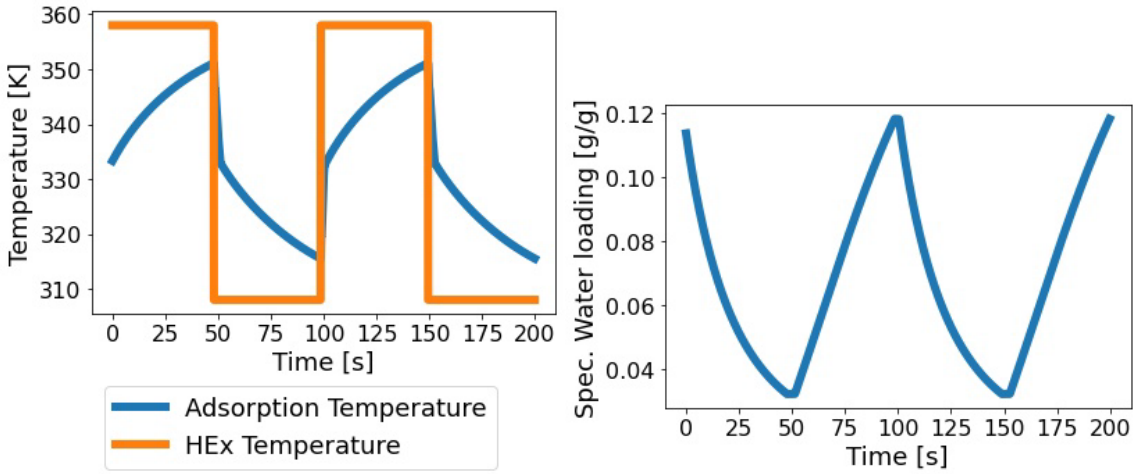

Figure 5 - Steady state cooling cycle for a 2 mm monolith. The adsorption temperature (left) increases fast due to the locality of the heat transfer. The adsorption on the materials (right) happens at a fast rate throughout the cycle.

4. Adsorption Heat and Mass Exchanger Characterization

For an adHP design in the power range of several kW, small-scale adsorber-desorber heat exchanger (A-D HEx) cyclic experiments around 1 kW open the possibility to investigate and optimize the HEX design. The design and manufacturing of the AC-based A-D HEx unit is one of the key tasks in the development of an adHP (Mohammadzadeh Kowsari et al., 2018). To characterize the A-D HEx efficiency, the sorbate mass is measured dynamically in-situ for both half cycles (adsorption and desorption). By knowing the dry mass and the adsorption potential (pressure/temperature conditions) in function of the sorbate loading on the adsorbent material, the adsorbed sorbate acts as a reference for the power (i.e. the external heat transfer loop efficiency).

In the adsorber - desorber characterization the mass uptake w(t) in the adsorption and mass loss in the desorption cycling is measured. The amount of w(t) multiplied by the heat of evaporation L of the sorbate is used as a benchmark for the efficiency of the heat and mass exchanger. L is a function of temperature T and in case of water L (20

°C) = 2537.5 kJ/kg (VDI-Wärmeatlas, Springer-Verlag Berlin Heidelberg 2013).

Therefore, the measurement setup of the SNF THRIVE project (Gantenbein et al., 2017) was modified. This comprised the modification of the external heat transfer fluid loops and additional sensors – like a new balance beam (HBK Plattformwägezelle 1-SP4MC6MR/7KG-1) of a higher resolution (mass m +/- Δm of 0.5 g).

Figure 6 shows the graphical user interface (GUI) of the NI LabVIEW data acquisition system. The principle of the setup with heat sources and heat sinks can be seen. Therefore, 3 thermostatic baths are used to perform adsorption and desorption (with the A/D HEX) as well as evaporation (evaporator) and condensation (condenser) of sorbate in the cycles. With a 4th thermostat the double jacked is thermostated to avoid heat transfer from and to the environment (the inner vacuum envelope surface) from and to the A/D HEX. In Figure 8 part of the open single chamber with the installed A/D HEX I (suspended at the beam balance) is shown and the right of this figure shows a section of the activated carbon sorbent disks stack.

Prior to cyclic adsorption and desorption measurements with sorbate, a calibration procedure without sorbate has to be performed for each cycle time t_{cycle}. These calibrations account for all "virtual" mass changes induced by thermal expansion of the A/D HEX, pressure oscillations in the heat transfer fluid and any heat input from the surrounding. Figure 7 shows weight measurement data for both adsorption and desorption. At the onset of adsorption (resp. desorption) the behaviour with a high mass uptake (resp. decrease) per time can be seen. In the curve fitting the coefficients a_l, d_k and the indices l, k have to be determined for each temperature quadruple and cycle time. After this procedure the functions can be used to parameterise a sorption heat pump model.

After the measurements with the sorbent-sorbate combination, an appropriate data procedure follows to determine the efficiency parameters. The power of the A/D HEX I was determined by the sorbate mass uptake w(t) and mass loss through the adsorption desorption cycles. Although the sorbent shows a high kinetic behavior (steep increase of the mass uptake at the onset of adsorption) a low power in the range of 100 W was reached (SCP: 300 W/kg) due to a long cycle time t_{cycle}. A close look to the mass curve w(t) indicates to shorten the t_{cycle} down to approx. one half – and therefore nearly a double of the SCP would be reached. An even higher SCP is expected with unaged sorbent material and an unaged A/D HEX (no peeling/dissolution of sorbent from the heat conduction Copper fins). In fact, the sorbent aging depends of the interaction with the sorbate and should not occur in normal operating conditions.

Based on the defined temperatures of the scenarios the sorbate vapor pressure p_s is in the range of 17.1 mbar (15 °C) and 42.5 (30 °C) sub-atmospheric pressures. The understanding of the sorption kinetics in the 1 kW power range allows for the scaling of results to a several kW (heating and cooling) power adsorption heat pump (Dague-net-Frick et al., 2017).

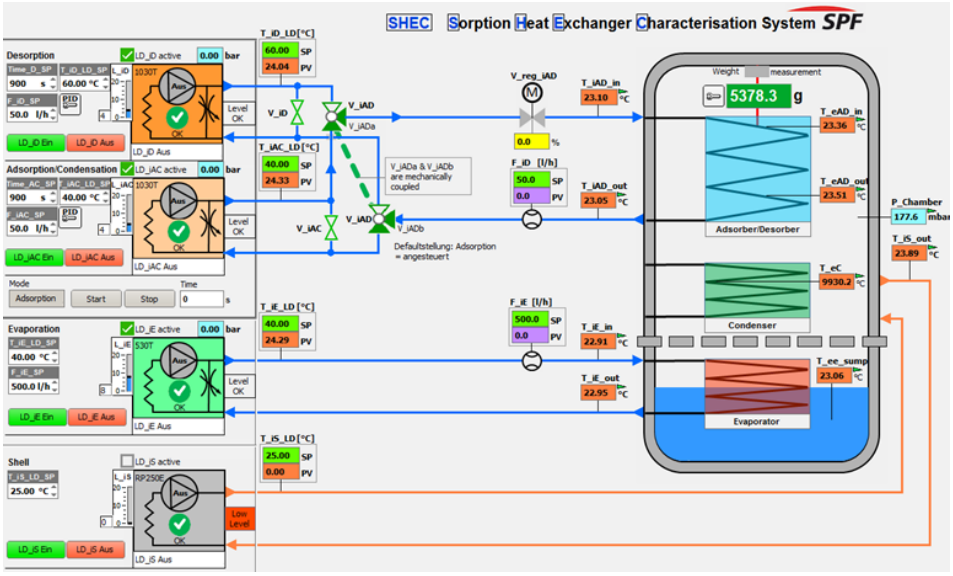

Figure 6 - graphical user interface (GUI) of the NI LabVIEW data acquisition system: 4 thermostatic baths as heat sources and heat sinks (left), single chamber setup with double jacket envelope and installed evaporator and adsorber/desorber (right), tubing and sensors. The original condenser is not installed – but the evaporator has a double function for evaporation and condensation.

Therefore, the evaporator is partly immersed in the liquid sorbate (blue color and temperature sensor T_ee_sump). While the lower part acts as an evaporator, the upper part acts as a condenser.

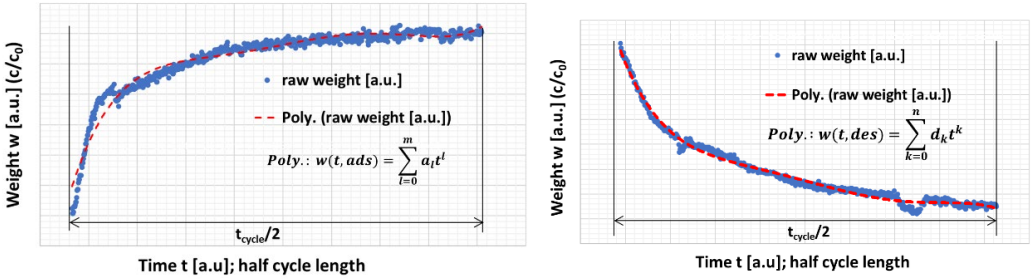

Figure 7 - Measurement data: adsorption (left) resp. desorption (right) curve over the half cycle time (a. u. = arbitrary units) and concept of data curve analysis with peace wise fit functions.

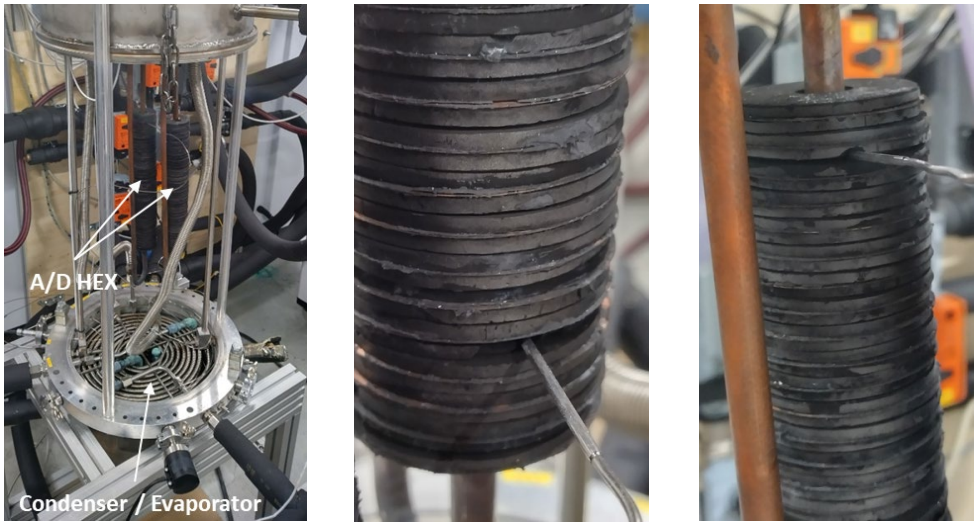

Figure 8 - SHEC and installed activated carbon sorbent disks stack: photo of the open single chamber measurement setup (left) and a section of the A/D HEX I with clamped Pt 100 temperature sensors (right). The sorbent disks sandwich the heat conducting Copper fins.

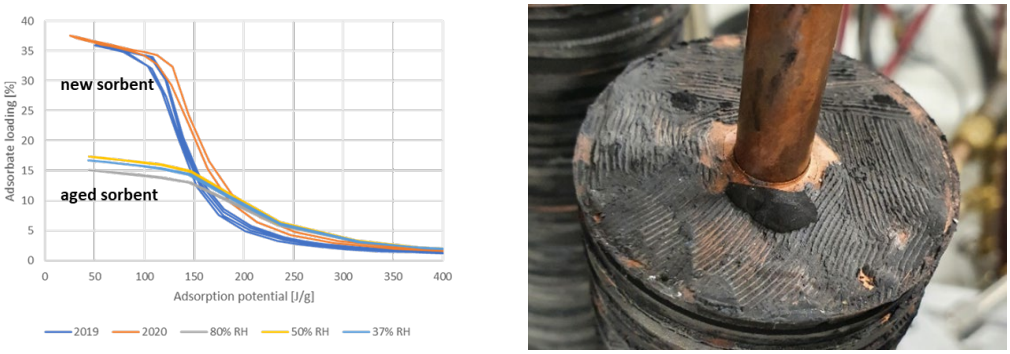

Figure 9 - sorbent ageing and peeling of the Copper fins: the sorbent shows an intrinsic ageing behavior after a 3 years exposure to sorbate vapor (left graph with the adsorbate loading in function of the age of the sorbent) and the sorbent disk peeled of the copper fin due to ageing of the glue (right picture).

5. Conclusions

In this work, we presented relevant progress obtained towards the design of adsorption heat pumps capable of improving district heating network efficiency in both heating and cooling mode. Firstly, the needs of DHN operators are examined and the most useful applications were selected. Specifically, in the heating mode the adHP can reduce the return temperature of the network, while in cooling mode the waste heat usage is increased.

The adsorbent material developed, an activated carbon (AC) obtained from spent coffee grounds, is a much more sustainable material than state-of-the-art ACs. The obtained adsorbent delivers satisfactory performance for the application studied. In particular, the pyrolysis process gives a good control over the adsorption characteristic curve, and should be further explored for sieved green body and towards higher temperatures and lower durations. Moreover, the models and the simulations of the AC gave useful insight on further development. Thin monoliths (<1mm) can be more performant than thicker ones, but they will be limited by the HEx design. Thicker monoliths are compatible with conventional HEx and are therefore very promising, as they provide a unique solution for effective HEx are usage.

Lastly, we built and tested a 1kW-prototype characterization setup with increased capacity and accuracy, which will be fundamental for further development of the adHP. In this setup, we could evaluate the effects of bad material handling and ageing.

6. Acknowledgments

We acknowledge the support of the Swiss Federal Office of Energy, as well as the contributions received from Juan Antonio Pérez López, Sahana Tavaragondi and Riccardo Torreggiani during their stay at Empa.

7. Nomenclature

Quantities

Quantity	Symbol	Unit	Quantity	Symbol	Unit
Specific heat	c	J/kg/K	Area	A	m^2
Thermal conductivity	k	W/m/K	Specific area	a	m^2/g
Diffusion coefficient	D	m^2/s	Enthalpy	h	J/kg
Sat. water capacity	W	g/g	Mass	m	kg
Char. ads. energy	C	J/ g	Heat	E	J
Thermal diffusivity	α	m^2/s	Mass flow rate	$\dot{m}$	kg/s
Ads. char. shape factor	N		Heat transf. resistance	R_{heat}	K/W
Porosity	ε		Heat flow rate	Q	W
Specific pore volume	v	cm^3/g	Mass transf. resistance	R_{mass}	s/m^3
Density	ρ	kg/m^3	Temperature	T	K
Time	t	s	Pressure	p	Pa
Adimensional time	τ		Gas concentration	γ	kg/m^3
Radius	r	m	Volume	V	m^3
Specific ads. loading	w	g/g	Thickness	s	m
Adsorption energy	H	J/kg	Adsorption energy	F	J/g
Evaporation enthalpy	L	J/kg			

Subscripts

Quantity	Symbol	Quantity	Symbol
Fin	f	Skeletal	$skel$
Saturation	sat	Adsorbate	a
Evaporator	eva	Adsorbent	s
Condenser	con	Vapour	v
Adsorption	ads	Macroscopic	M
Hot source	hot	Microscopic	μ
Internal	int	Mesoscopic	m
External	ext	Initial	i
Envelope	env		

8. References

Alshrah, M., Tran, M.-P., Gong, P., Naguib, H.E., Park, C.B., 2017. Development of high-porosity resorcinol formaldehyde aerogels with enhanced mechanical properties through improved particle necking under CO 2 supercritical conditions. Journal of Colloid and Interface Science 485, 65–74. https://doi.org/10.1016/j.jcis.2016.09.030

Ammann, J., Michel, B., Ruch, P.W., 2019. Characterization of transport limitations in SAPO-34 adsorbent coatings for adsorption heat pumps. International Journal of Heat and Mass Transfer 129, 18–27. https://doi.org/10.1016/j.ijheatmasstransfer.2018.09.053

Birol, D.F., 2018. The Future of Cooling 92.

Carslaw, H.S., Jaeger, J.C., 1959. Conduction of Heat in Solids, 2nd ed. Oxford University Press, Great Britain.

Civioc, R., Lattuada, M., Koebel, M.M., Galmarini, S., 2020. Monolithic resorcinol–formaldehyde alcogels and their corresponding nitrogen-doped activated carbons. J Sol-Gel Sci Technol 95, 719–732. https://doi.org/10.1007/s10971-020-05288-x

Daguenet-Frick, X., Moullet, Y., Gantenbein, P., Persdorf, P., Notter, D., 2017. Adsorption Heat Pump Upscaling from 1 KW to 10 KW of Cooling Power: Experimental Based Modelling, in: International Sorption Heat Pump Conference 2017. Presented at the International Sorption Heat Pump Conference 2017, Tokyo.

Dubinin, M.M., Astakhov, V.A., 1971. Development of the concepts of volume filling of micropores in the adsorption of gases and vapors by microporous adsorbents 5.

Gantenbein, P., Daguenet-Frick, X., Bont, F., Persdorf, P., Notter, D., 2017. Cooling power determination by measuring the adsorbed vapor mass variations: comparison of mass adsorption cooling power correlation and external fluid loop power measurement, in: International Sorption Heat Pump Conference 2017. Presented at the International Sorption Heat Pump Conference 2017, Tokyo.

Hassan, A.A., Elwardany, A.E., Ookawara, S., Ahmed, M., El-Sharkawy, I.I., 2020. Integrated adsorption-based multigeneration systems: A critical review and future trends. International Journal of Refrigeration 116, 129–145. https://doi.org/10.1016/j.ijrefrig.2020.04.001

Huber, L., Hauser, S.B., Brendlé, E., Ruch, P., Ammann, J., Hauert, R., Widmer, R.N., Ubert, C.J., Matam, S.K., Yoon, S., Zhang, Y., Koebel, M.M., 2019. The effect of activation time on water sorption behavior of nitrogen-doped, physically activated, monolithic carbon for adsorption cooling. Microporous and Mesoporous Materials 276, 239–250. https://doi.org/10.1016/j.micromeso.2018.09.025

Huber, L., Ruch, P., Hauert, R., Matam, S.K., Saucke, G., Yoon, S., Zhang, Y., Koebel, M.M., 2016. Water sorption behavior of physically and chemically activated monolithic nitrogen doped carbon for adsorption cooling. RSC Adv. 6, 80729–80738. https://doi.org/10.1039/C6RA18660B

Jobard, X., Padey, P., Guillaume, M., Duret, A., Pahud, D., 2020. Development and Testing of Novel Applications for Adsorption Heat Pumps and Chillers. Energies 13, 615. https://doi.org/10.3390/en13030615

Mohammadzadeh Kowsari, M., Niazmand, H., Tokarev, M.M., 2018. Bed configuration effects on the finned flat-tube adsorption heat exchanger performance: Numerical modeling and experimental validation. Applied Energy 213, 540–554. https://doi.org/10.1016/j.apenergy.2017.11.019

Nowicki, P., Pietrzak, R., Wachowska, H., 2010. Sorption properties of active carbons obtained from walnut shells by chemical and physical activation. Catalysis Today 150, 107–114. https://doi.org/10.1016/j.cattod.2009.11.009

Olivier, J.P., 1995. Modeling physical adsorption on porous and nonporous solids using density functional theory. J. Porous Mater. 2, 9–17.

Piccoli, E., Frazzica, A., Galmarini, S., 2021. D4.3: Model capable of estimating the performance of a given adsorption chiller set-up and a given adsorber material for a given application scenario, Hycool project public deliverables.

Prauchner, M.J., Rodríguez-Reinoso, F., 2012. Chemical versus physical activation of coconut shell: A comparative study. Microporous and Mesoporous Materials 152, 163–171. https://doi.org/10.1016/j.micromeso.2011.11.040

Puschnigg, S., Jauschnik, G., Moser, S., Volkova, A., Linhart, M., 2021. A review of low-temperature sub-networks in existing district heating networks: examples, conditions, replicability. Energy Reports 7, 18–26. https://doi.org/10.1016/j.egyr.2021.09.044

Quiquerez, L., 2017. Décarboner le système énergétique à l'aide des réseaux de chaleur: état des lieux et scénarios prospectifs pour le canton de Genève. https://doi.org/10.13097/ARCHIVE-OUVERTE/UNIGE:93380

Settembrini, G., Domingo-Irigoyen, S., Heim, T., Jurt, D., Zakovorotnyi, A., Seerig, A., Zweifel, G., Menti, U.P., 2017. ClimaBau - Planen angesichts des Klimawandels. Lucerne University of Applied Sciences and Arts.

Stahl, Th., Brunner, S., Zimmermann, M., Ghazi Wakili, K., 2012. Thermo-hygric properties of a newly developed aerogel based insulation rendering for both exterior and interior applications. Energy and Buildings 44, 114–117. https://doi.org/10.1016/j.enbuild.2011.09.041

Tarazona, P., 1985. Free-energy density functional for hard spheres. Physical Review A 31, 2672.